Kitaev interactions of the spin-orbit coupled magnet UO2

Joseph Paddison, Lionel Desgranges, Gianguido Baldinozzi, G Lander, Henry Edward Fischer

Kitaev interactions of the spin-orbit coupled magnet UO_2

Joseph A. M. Paddison,[1,*] Lionel Desgranges,[2] Gianguido Baldinozzi,[3] Gerard H. Lander,[4] and Henry E. Fischer[4,†]

[1]*Neutron Scattering Division, Oak Ridge National Laboratory, Oak Ridge, Tennessee 37831, USA*
[2]*CEA.DES.IRESNE.DEC, Cadarache F 13108 St Paul Lez Durance, France*
[3]*Centralesupélec, Centre National de la Recherche Scientifique, Structures Property and Modeling of Solids Laboratory, Université Paris-Saclay, Gif-sur-Yvette 91190, France*
[4]*Institut Laue-Langevin, 71 avenue des Martyrs, CS 20156, 38042 Grenoble cedex 9, France*

Uranium dioxide, UO_2, is a canonical example of a magnetic material with strong spin-orbit coupling. Here, we present a study of the magnetic diffuse scattering measured on a polycrystalline sample of UO_2, which we interpret in terms of its magnetic interactions between U^{4+} magnetic moments. By refining values of the magnetic interaction parameters to magnetic diffuse-scattering data measured above the magnetic ordering transition temperature, we show that the dominant magnetic coupling in UO_2 is a bond-dependent interaction analogous to the Kitaev model of honeycomb magnets. We compare our experimental results with published theoretical predictions and experimental measurements of the magnetic excitation spectrum. Our results suggest that magnetic materials with f-electron magnetic ions, particularly actinides, may be promising candidates for realising Kitaev magnetism, and highlight the role that magnetic diffuse-scattering data can play in identifying such materials.

The Heisenberg model of isotropic magnetic interactions is among the most important models in magnetism [1]. Recently, however, there has been renewed interest in magnetic interactions that deviate from the isotropic Heisenberg limit and are strongly bond-dependent. This interest has been motivated by the theoretical discovery of a topological spin-liquid ground state for the Kitaev model on the honeycomb lattice [Figure 1(a)], which provides a foundational example of bond-dependent magnetism [2, 3] that has potential applications in quantum computing [4]. Subsequently, the Kitaev model has been generalized to other lattices [5, 6], including triangular, pyrochlore and face-centred cubic [Figure 1(b)]. While these lattices do not show equivalent ground states to the honeycomb Kitaev model, they can nevertheless exhibit many unusual magnetic properties, including spin-liquid behaviour [7, 8] and multipolar excitations [9]. Moreover, identifying Kitaev materials on any lattice can help to understand the factors that enhance the Kitaev interaction [10]. Consequently, identifying materials where Kitaev interactions are dominant is an important goal in condensed-matter physics.

A key ingredient to stabilise large Kitaev interactions is spin-orbit coupling, which is enhanced for heavier magnetic elements. Motivated by this observation, we decided to re-examine the magnetic interactions of uranium dioxide, UO_2. Uranium dioxide has been extensively studied due to its use as a nuclear-fuel material at high temperatures [11, 12], but it is also of fundamental interest due to its low-temperature properties [13]. At low temperatures, strong coupling of spin, orbital and lattice degrees of freedom has been revealed by the observation of mixed magnon-phonon excitations [14–16], and by magnetoelastic responses with potential applications in magnetic sensing [17, 18]. Uranium dioxide crystallises in the fluorite structure (space group $Fm\bar{3}m$; $a = 5.46$ Å) [19], where U^{4+} ions occupy a face-centred cubic lattice. A first-order transition to an antiferromagnetic state occurs at $T_N = 30.8$ K [20, 21]. The small value of T_N compared to the antiferromagnetic Weiss temperature $\theta \sim -220$ K [22] suggests that magnetic interactions are frustrated. In the antiferromagnetic state, the magnetic propagation vector $\mathbf{k} = [001]$. While neutron-diffraction experiments were initially interpreted in terms of a single-$\mathbf{k}$ antiferromagnet with the spin direction transverse to $\mathbf{k}$ [23], subsequent measurements established that the magnetic ground state is actually a transverse triple-$\mathbf{k}$ structure [24] that can be described by a superposition of the spin orientations within single-$\mathbf{k}$ domains [Figure 1(c)].

To explain the properties of UO_2, a theoretical framework has been developed that includes crystal-field effects and interactions between dipolar and quadrupolar degrees of freedom [15, 16, 25–27]. The crystal-field ground state is a triplet that is separated from the first excited state by approximately 150 meV [28–31], so that below room temperature, the magnetic moments can be modelled with an effective spin quantum number $S = 1$. This has two important implications for the magnetic Hamiltonian. First, axial single-ion anisotropies are not allowed in a cubic environment for any S, and an effective $S < 2$ also prohibits "cubic" single-ion anisotropy terms [32]. Consequently, no single-ion anisotropy is expected in UO_2. Second, an effective $S = 1$ carries both dipolar and quadrupolar degrees of freedom; e.g., the $S_z = 0$ state carries a quadrupole moment but no dipole moment [9]. Although excitations of purely quadrupolar degrees of freedom are silent in neutron-scattering measurements, it proved possible to observe hybridised dipolar-quadrupolar excitations in UO_2 [15, 16], and these measurements yielded deep insights into the exchange interactions of both dipolar and quadrupolar origin. Due to the complexity of the low-temperature excitation spectrum, however, a direct refinement of the magnetic interactions to experimental data has not yet been available.

Here, we report experimentally-derived values of the magnetic exchange interactions in UO_2 based on fits to magnetic diffuse-scattering data measured on a polycrystalline sample above T_N. We find that the magnetic diffuse scattering data cannot be described by an isotropic Heisenberg model; instead, a good description of our data requires a large Kitaev interaction. Our fitted values of the dipolar interactions are in qualitative agreement with the most recent theoretical predic-

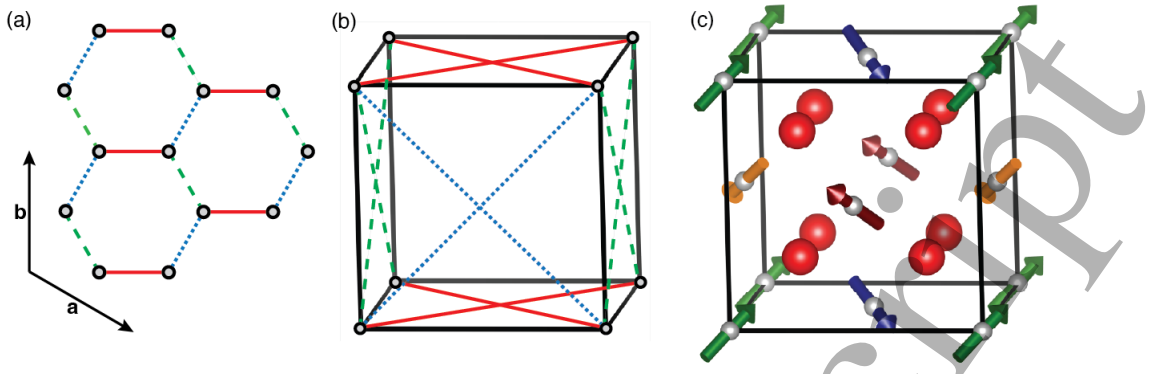

Figure 1. (a) Kitaev model on the honeycomb lattice. (b) Kitaev model on the face-centered cubic lattice. In (a) and (b), the Kitaev interaction couples the z components of spins connected by red solid lines, the x components of spins coupled by the green dashed lines, and the y components of spins coupled by the blue dotted lines. (c) Transverse triple-**k** magnetic structure of UO_2, showing U^{4+} ions as grey spheres, O^{2-} ions shown as red spheres, and spin directions as arrows. Different colours of the spins are used to show the four $\langle 111 \rangle$ directions along which spins are aligned in this non-coplanar magnetic structure.

tions [25, 26]. We discuss our results in the context of the low-temperature excitation spectra [14], and compare UO_2 with other materials that realize bond-dependent magnetism on the FCC lattice.

Our UO_2 sample was comprised of two cylindrical polycrystalline ingots, each of dimensions 8.3 mm in diameter and 14 mm in height, stacked on top of each other within a sealed thin-walled vanadium sample container of diameter 9 mm. The two UO_2 ingots were obtained by sintering at 1970 K under a 5% Ar/H_2 atmosphere, and contained about 0.1 mol.% impurities. Neutron diffraction data [33] were measured at temperatures between 10 and 300 K using the D4 instrument [34] at the Institut Laue-Langevin (Grenoble, France) with incident wavelength $\lambda = 0.5$ Å, providing a maximum wavevector transfer of $Q_{\max} = 23.5$ Å^{-1} that is sufficient for a good-quality Fourier transform to a pair-distribution function PDF(r). Using a short neutron wavelength ensures that the magnetic scattering is integrated over a wide energy range, yielding an accurate estimate of the equal-time spin correlations; however, it also relaxes the Q-resolution, resulting in relatively broad nuclear Bragg peaks. With these effects in mind, the data were processed as follows. First, each data set was normalised in absolute intensity units (barn/sr/U) using the limiting values of the pair-distribution function. It was necessary to normalise each data set independently, due to thermal-expansion effects that caused the quantity of sample exposed to the beam to vary slightly with temperature. Second, to isolate the magnetic scattering arising from the development of spin correlations below room temperature, a 300-K data set was subtracted from every other data set. When performing these subtractions, we accounted for temperature-dependent changes in lattice parameter by rescaling the Q-axis, and changes in thermal motion by dividing the data by the Debye-Waller factor and subtracting the thermal diffuse scattering (TDS), using Rietveld refinements to obtain initial estimates of lattice parameters and Debye-Waller factors, and fits of the high-Q region to a Q^2 intensity dependence to estimate the TDS. This process allowed for a relatively clean subtraction of the nonmagnetic signals, except in the vicinity of the most intense nuclear Bragg scattering, where it was necessary to exclude some data points.

The magnetic diffuse scattering data measured above T_N are shown in Figure 2(a,b). They show the development of a peak centred around 1 Å^{-1} as the sample is cooled from room temperature to just above T_N, indicating the development of antiferromagnetic correlations with an increasing coherence length. These data were previously published [35] and analysed using the reverse Monte Carlo method [36], revealing antiferromagnetic correlations with magnitudes consistent with a theoretical study [26]. The magnetic diffuse scattering can be directly related to the exchange interactions by applying a reaction-field approximation [37–40]. For a structure such as UO_2, which has a single magnetic atom in its primitive unit cell, the Fourier transform of the magnetic interactions is written as a 3×3 matrix $\mathsf{J}(\mathbf{Q})$ with elements $J_{\alpha\beta}(\mathbf{Q}) = -\sum_{\mathbf{R}} J_{\alpha\beta}(\mathbf{R}) e^{-i\mathbf{Q}\cdot\mathbf{R}}$, where α, β are Cartesian spin components, and $J_{\alpha\beta}(\mathbf{R})$ is the coefficient of $S_i^\alpha S_j^\beta$ in Eq. (2), for pair of spins i, j that are separated by a primitive lattice vector $\mathbf{R}$. The interaction matrix is diagonalised to obtain its eigenvalues $\lambda_\mu(\mathbf{Q})$ and eigenvector components $U_\mu^\alpha(\mathbf{Q})$. The magnetic diffuse scattering intensity is obtained as

$$I(\mathbf{Q}) = C\frac{[\mu_{\text{eff}} f(Q)]^2}{3} \sum_{\mu=1}^{3} \frac{|\mathbf{s}_\mu^\perp(\mathbf{Q})|^2}{1 - \chi_0 [\lambda_\mu(\mathbf{Q}) - \lambda]}, \qquad (1)$$

where μ_{eff} is the magnetic moment per ion, $C = 0.07265$ barn, $f(Q)$ is the U^{4+} magnetic form factor given in Ref. [41], $\chi_0 = 1/3T$ is the Curie susceptibility, and for the FCC lattice $\mathbf{s}_\mu^\perp(\mathbf{Q}) = \sum_{\alpha=1}^{3} (\hat{\mathbf{n}}_\alpha - \mathbf{Q}\hat{\mathbf{n}}_\alpha \cdot \mathbf{Q}/Q^2) U_\mu^\alpha(\mathbf{Q})$, where $\hat{\mathbf{n}}_\alpha$ is a unit vector parallel to $\mathbf{x}, \mathbf{y}$, or $\mathbf{z}$ [39, 40]. Magnetic diffuse scattering calculations were performed using the Spinteract program [40], which numerically powder averages Eq. (1) and convolves the result with the instrumental resolution function of D4. This procedure allows for a quantitative comparison of

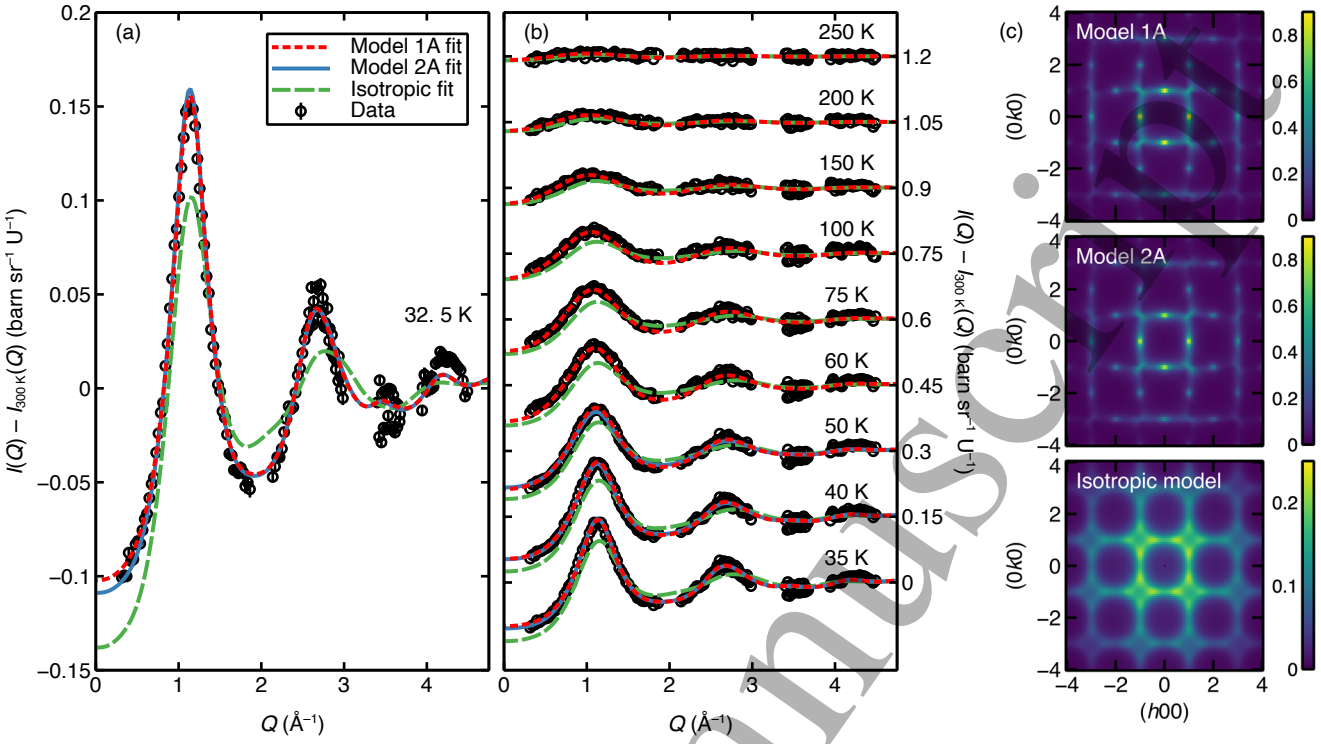

Figure 2. Magnetic diffuse scattering data (black circles) and model fits (lines), showing (a) 32.5 K data only, and (b) data measured at 35 K to 250 K, with successive temperatures vertically offset by 0.15 units for clarity. Temperatures are labelled above each curve and a data set measured at 300 K has been subtracted from every data set shown. Green dashed lines show model fits to all data for isotropic interactions up to fourth neighbours, allowing an intensity scale factor to vary separately for each data set. Red dotted lines show model fits to all data for the J-K-Γ-J_3 model (Eq. (3)), allowing an intensity scale factor to vary separately for each data set (Model 1A in Table I). Blue solid lines show model fits to data measured between 32.5 K and 50 K for the J-K-Γ-J_3 model (Eq. (3)), allowing a common intensity scale factor for all data sets (Model 2A in Table I). Fits for Model 2A and Model 2B resemble fits for Model 1A and Model 1B, respectively, and are not shown. (c) Calculated single-crystal magnetic diffuse scattering intensity in the $(hk0)$ plane for Model 1A, Model 2A, and the isotropic model. The color scale shows scattering intensity $I(\mathbf{Q})$ calculated within the Onsager reaction-field framework at $T = 32.5$ K.

the calculated diffuse scattering patterns with our experimental data.

As a first attempt to analyse these data in terms of the magnetic Hamiltonian, we considered the isotropic Heisenberg model,

$$H_{\rm iso} = \sum_{\langle i,j\rangle \in n} J_n \mathbf{S}_i \cdot \mathbf{S}_j, \qquad (2)$$

where J_n is the isotropic exchange interaction between n-th neighbours, and we employ the conventions that antiferromagnetic interactions have positive sign, each pairwise interaction is counted once, and the spins are classical vectors of length $\sqrt{S(S+1)} = \sqrt{2}$. We attempted to refine the values of isotropic interactions up to fourth neighbors against the data collected between 31 and 250 K simultaneously. Figure 2 shows a comparison of our experimenal data with the best fit for this model. The isotropic model does not describe the data well, since it fails to capture the shape of the main diffuse peak at temperatures below 150 K. In the refinements shown, an overall intensity scale factor was allowed to refine independently for each data set; hence, the disagreement cannot be addressed by a simple scaling of the fitted curves. Attempts to refine additional parameters—including magnetic interaction parameters up to $n = 7$—also failed to produce a meaningful improvement in the fit quality. We conclude from this that our data cannot be explained by an isotropic model.

We therefore consider a more general Hamiltonian that contains all nearest-neighbour interactions allowed by the space-group symmetry of UO_2, but is restricted to only bilinear interactions; i.e., those that are linear in components of each spin. This Hamiltonian can be written as

$$H_{\rm bd} = \sum_{\langle i,j\rangle \in n} J_n \mathbf{S}_i \cdot \mathbf{S}_j + K \sum_{\langle i,j\rangle_\gamma} S_i^\gamma S_j^\gamma + \Gamma \sum_{\langle i,j\rangle_\gamma} \left(S_i^\alpha S_j^\beta + S_i^\beta S_j^\alpha \right), \qquad (3)$$

where the bond-dependent interactions are K (the Kitaev interaction) and Γ [42–44]. The notation $\langle i,j\rangle_\gamma$ indicates that the sum runs over pairs of U^{4+} ions in the plane perpendicular to the γ-axis; for example, if we consider a pair of U^{4+} ions within the xy plane, then the Kitaev term couples their z components $S_i^z S_j^z$, whereas the Γ term couples their x and y spin components, $S_i^x S_j^y + S_i^y S_j^x$. The corresponding $\mathrm{J}(\mathbf{Q})$ is

given explicitly in Ref. [42].

Theoretical studies have shown that bond-dependent couplings are important in determining the magnetic ground state on the FCC lattice [42, 43]. For UO_2, Heisenberg interactions are antiferromagnetic ($J > 0$); this supports antiferromagnetic ordering with $\mathbf{k} = [100]$, as is observed experimentally. In this regime, the sign of the Kitaev term plays a central role in determining the specific ground state [42, 43]. Positive values of K stabilise a ground state with the spin direction perpendicular to $\mathbf{k}$, whereas negative values of K stabilise a ground state with spins parallel to $\mathbf{k}$. The effect of Γ on the ground state is more subtle, but $\mathbf{k} = [100]$ ordering remains stable for $K < 0$ and relatively small $|\Gamma| \lesssim K$. An unusual feature of the Hamiltonian defined by Eq. (3) is that single-$\mathbf{k}$ and triple-$\mathbf{k}$ structures are energetically degenerate for any choice of J, K and Γ that stabilises magnetic ordering with $\mathbf{k} = [100]$ [43, 44]. This implies that further interactions are required to stabilise the triple-$\mathbf{k}$ ordering observed in UO_2. We will return to this point below.

Figure 2(a,b) shows fits to our neutron data allowing four interaction parameters to vary—J, K, Γ, and an isotropic third-neighbour coupling J_3. Excellent agreement is now obtained for this model—which contains the same number of free parameters as the isotropic model considered above—suggesting that anisotropic interactions are important in UO_2. Initially, we allowed an overall intensity scale factor to refine independently for each data set; the values obtained indicated a significant temperature dependence of the effective magnetic moment, from approximately $2.0\,\mu_B$ at 31 K to $2.9\,\mu_B$ at 250 K, which may be related to thermal population of excited crystal-field levels. A reasonable refinement could be achieved with a common scale factor for data collected between 31 and 50 K, so a second set of refinements was performed over this restricted temperature range. Refinements were also performed allowing the isotropic next-nearest-neighbour coupling J_2 to vary instead of J_3. For each model, Table I presents the fitted parameter values, the sum of squared residuals R_{wp}, and the calculated magnetic ordering temperature T_N^{calc}, which is obtained in the reaction-field approximation following Ref. [38]. The difference in the magnetic diffuse scattering between isotropic and anisotropic models is even more apparent in calculations of the single-crystal diffuse scattering intensity, which are shown for each model in Figure 2(c) and show much sharper features for the anisotropic model than the isotropic one at the same temperature.

We now discuss the physical implications of the results given in Table I. While different refinement protocols yielded significant differences in the refinement parameter values, several conclusions can be reached. Most importantly, the Kitaev interaction is always positive and is the largest term, with a magnitude at least double that of any other interaction. A key result of our work is therefore that K provides the dominant energy scale in UO_2. The positive sign of K is consistent with the observed transverse magnetic structure [43]. The next-largest interaction is Γ, which our refinements show to have a negative value. The Heisenberg interaction is antiferromagnetic, as anticipated, but significantly smaller than K. The further neighbour couplings are the smallest terms, and our data are nearly equally well described by a small ferromagnetic J_2 (models 1B, 2B) or antiferromagnetic J_3 (models 1A, 2A). Either of these possibilities can help to stabilise $\mathbf{k} = [100]$ ordering, as observed experimentally, whereas the opposite choice of signs (ferromagnetic J_3 or antiferromagnetic J_2) would stabilise ordering with $\mathbf{k} = [1\frac{1}{2}0]$ [43]. The calculated magnetic ordering temperatures are typically around 20 K, which is a significant ($\sim$30%) underestimate compared to the experimental value of 30.8 K. This may be due to the use of the reaction-field approximation, which can underestimate magnetic ordering temperatures by up to $\sim$20% [45]. It may also occur because the magnetic transition in the real material is first-order and driven by quadrupolar interactions, which are not considered in Eq. (3). Overall, the results shown in Table I suggest the following range of values for the interaction parameters: $2 \lesssim J \lesssim 6$ K, $14 \lesssim K \lesssim 20$ K, $-9 \lesssim \Gamma \lesssim -6$ K, $-0.7 \lesssim J_2 \lesssim 0$ K, and $0 \lesssim J_3 \lesssim 0.2$ K.

Estimates of all the magnetic interactions in Eq. (3) have been reported from theory, and some terms have also been previously estimated experimentally. Our results are consistent with the values of J and K estimated in a neutron spectroscopy study, in which Γ was not reported [16]. A detailed comparison with early inelastic scattering work [46] is not possible due to its assumption of a single-$\mathbf{k}$ structure, but the overall energy scales we identify are qualitatively consistent. Our results are also in remarkably good agreement with a recent first-principles study [26], showing the same signs and similar magnitudes of J, K, and Γ. Agreement in the relative magnitudes of J and K is also obtained with an independent theoretical study [25]. Our experimental analysis therefore provides strong support for the theoretical results of Refs. [25, 26].

Magnetic diffuse-scattering data are primarily sensitive to bilinear interactions [9]. This has the advantage of simplifying the estimation of the bilinear terms; however, it is important to investigate how the neglect of quadrupolar interactions affects the values of the bilinear terms obtained in this way. To do so, we note that quadrupolar interactions are biquadratic when expressed in terms of spin components, and consider the simplest case of isotropic nearest-neighbour biquadratic interactions,

$$H_{bq} = J_{bq} \sum_{\langle i,j \rangle} (\mathbf{S}_i \cdot \mathbf{S}_j)^2, \tag{4}$$

where J_{bq} denotes the biquadratic exchange coupling. This is the lowest-order interaction that can remove the degeneracy between single-$\mathbf{k}$ and triple-$\mathbf{k}$ structures: positive values of J_{bq} stabilise triple-$\mathbf{k}$ ordering, whereas negative values of J_{bq} stabilise single-$\mathbf{k}$ ordering [44]. In a mean-field approximation, J_{bq} has an equivalent effect on the magnetic diffuse scattering as an isotropic Heisenberg exchange term [47]; hence, a biquadratic coupling shifts fitted values of J. Specifically, the values of J given in Table I can be interpreted as $J = J_{true} - \frac{1}{2}J_{bq}$, where J_{true} is the true isotropic bilinear cou-

	J (K)	K (K)	Γ (K)	J_2 (K)	J_3 (K)	$R_{\rm wp}$ (%)	$T_{\rm N}^{\rm calc}$ (K)	$\mu_{\rm eff}$ ($\mu_{\rm B}$)
Model 1A (independent scale, $T \leq 250$ K)	2.4(2)	19.3(3)	−9.0(3)	0*	0.13(2)	19.8	19.5	2.01 - 2.88
Model 1B (independent scale, $T \leq 250$ K)	2.5(2)	17.6(3)	−8.4(2)	−0.6(1)	0*	19.7	20.0	2.03 - 2.96
Model 2A (common scale, $T \leq 50$ K)	5.6(2)	14.5(3)	−7.1(2)	0*	0.15(2)	15.4	19.3	2.08
Model 2B (common scale, $T \leq 50$ K)	5.3(2)	13.8(3)	−6.6(2)	−0.3(1)	0*	15.5	16.2	2.11
Theory (Ref. [26])	8.2	14.1	−3.9	+0.8	0*			
Theory (Ref. [25])	3.0	6.9	0*	0*	0*			
Experiment (Ref. [16])	4.5	13.5	0*	0*	0*			

Table I. Refined interaction parameter values, sum of squared residuals $R_{\rm wp}$, calculated magnetic ordering temperature $T_{\rm N}$, and calculated effective paramagnetic moment $\mu_{\rm eff}$. Literature results are shown for comparison, which are reproduced from Ref. [26] and converted to match the convention of Eq. (3). Values denoted with an asterisk (*) were fixed during the refinements.

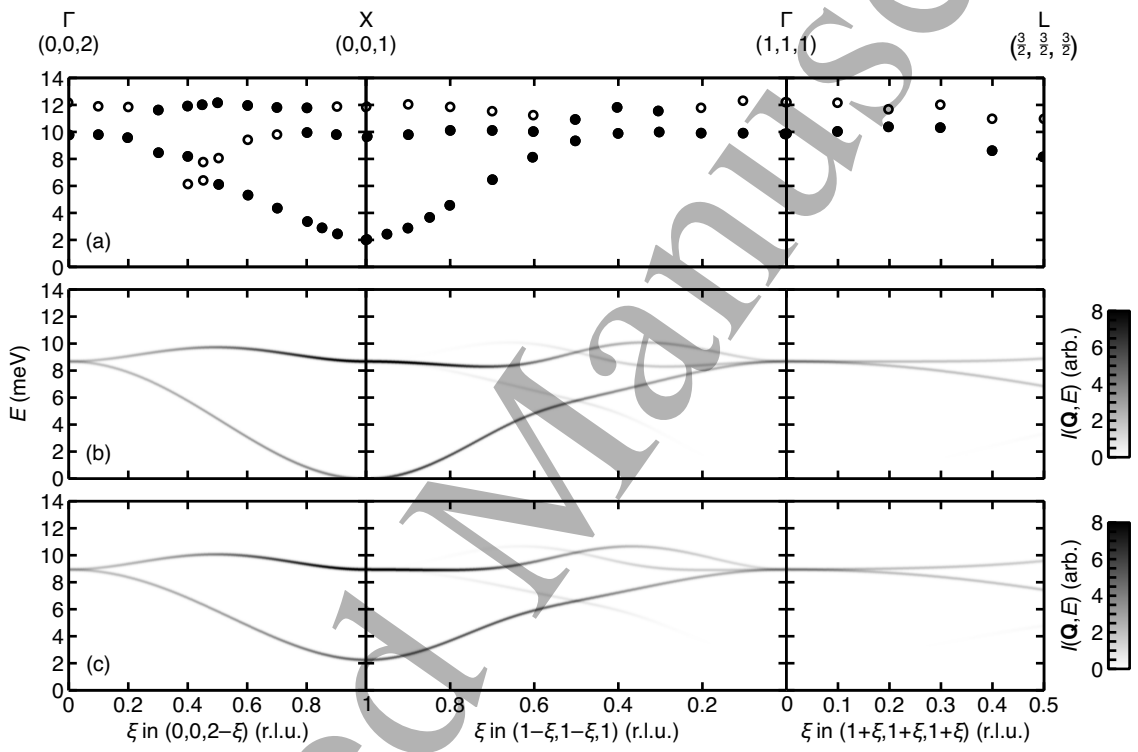

Figure 3. Magnetic excitations in UO_2, where r.l.u. denotes reciprocal-lattice units. (a) Previously published dispersion relation for UO_2, reproduced from Ref. [14]. Filled and empty circles indicate more and less intense modes, respectively. (b) Calculated inelastic neutron-scattering intensity for the J-K-Γ-J_3 model (Model 1A in Table I). (c) Calculated inelastic neutron-scattering intensity for the same model as (b), except a biquadratic interaction $J_{\rm bq} = 10$ K is assumed.

pling [47].

As a check on our results, we calculated the magnetic excitation spectrum for our model parameters using the SpinW program [48], and compared the result with published inelastic-neutron-scattering measurements of Ref. [14]. Figure 3(a) shows the published dispersion relation [14], which shows a minimum at the X = (001) point with a gap of ≈ 2 meV, and a large gap of ≈ 10 meV at the $\Gamma = (002)$ point. Figure 3(b) shows the calculated spin-wave spectrum for the J-K-Γ-J_3 model (Model 1A in Table I), assuming $S = 1$ and the transverse triple-**k** magnetic ground state. The calculation captures the overall shape of the dispersion curve, including a minimum at the X point and a large gap at the Γ point. This result points to a large Kitaev term, since for $K = 0$, there would be no gap at the Γ point, in strong disagreement with the data. The model also predicts the observed approximately quadratic spin-wave dispersion around the X point, which is uncommon for an antiferromagnet. However, the calculation deviates from the data in several respects: it shows a gapless spectrum in contrast to the observed ≈ 2 meV gap at the X point, the overall bandwidth is too small, and some weaker modes and splittings at high energy are not reproduced. The first of these discrepancies can be addressed by including a nonzero value of $J_{\rm bq}$. Figure 3(c) shows the calculated spin-

wave spectrum assuming $J_{bq} = 10\,\mathrm{K}$, which now reproduces the observed gap. We note that semiclassical spin-wave calculations require the use of renormalised or shifted values of J_{bq} and J to obtain correct results [49], which have been included in our calculation. Our results therefore suggest a substantial biquadratic interaction of the same order of magnitude as K. The $\sim$2 meV discrepancy in overall bandwidth and omission of weak high-energy modes may be related to the omission of anisotropic quadrupolar interactions and magnon-phonon couplings [16, 50], which are beyond the scope of our work focusing on the bilinear exchange interactions.

Our study highlights the surprising observation that magnetic diffuse-scattering data measured on polycrystalline samples are sensitive to bond-dependent interactions such as the Kitaev coupling [39]. In UO_2, our results indicate a dominant Kitaev interaction and smaller but still substantial Γ interaction. The presence of frustrated couplings supports a large temperature range where the system is a correlated paramagnet, where structured magnetic excitations may affect the thermal conductivity [51]. The anisotropic terms in UO_2 are much larger than those in FCC magnets where the magnetic ion is a transition metal. For example, the cubic double perovskites Ba_2YRuO_6 and Ba_2LuRuO_6 with magnetic Ru^{5+} ions ($4d^3$) were recently shown to have the same transverse triple-**k** ground state as UO_2, but the ratio $K/J \sim 0.02$ is two orders of magnitude smaller in these double perovskites than in UO_2 [44]. In K_2IrCl_6, in which Ir^{4+} moments ($5d^5$) also occupy a FCC lattice and $\mathbf{k} = [1, \frac{1}{2}, 0]$ is stabilised by fluctuations, $K/J \sim 0.2$ is still an order of magnitude smaller than in UO_2 [52]; a similar ratio has been calculated for Ba_2CeIrO_6 [53]. By contrast, the $4f$-electron magnets CeAs and CeSb have $|K/J| \sim 1.6$, and USb has a very large ratio $|K/J| \sim 10$ [54]. Taken together with our results for UO_2, these observations suggest that materials with magnetic f-electron elements may be the most promising systems to obtain a dominant Kitaev interaction. This goal remains relevant for lattices such as honeycomb, where a topologically-nontrivial spin-liquid ground state can only be realized if the Kitaev term dominates. Candidate materials such as α-$RuCl_3$ have been extensively investigated with the goal in mind, but recent results suggest that the non-Kitaev interactions are probably substantial [55]; hence, the search for ideal Kitaev honeycomb materials continues.

Work of J.A.M.P. (data analysis and manuscript writing) was supported by the U.S. Department of Energy, Office of Science, Basic Energy Sciences, Materials Sciences and Engineering Division.

* paddisonja@ornl.gov
† fischer@ill.fr

[1] R. Skomski, *Simple Models of Magnetism* (Oxford University Press, 2008).
[2] A. Kitaev, *Ann. Phys.* **303**, 2 (2003).
[3] I. Rousochatzakis, Y. Sizyuk, N. B. Perkins, *Nature Communications* **9**, 1575 (2018).
[4] G. Baskaran, S. Mandal, R. Shankar, *Phys. Rev. Lett.* **98**, 247201 (2007).
[5] I. Kimchi, A. Vishwanath, *Phys. Rev. B* **89**, 014414 (2014).
[6] J. Chaloupka, G. Khaliullin, *Phys. Rev. B* **92**, 024413 (2015).
[7] Y. Kato, Y. Kamiya, J. Nasu, Y. Motome, *Phys. Rev. B* **96**, 174409 (2017).
[8] P. Kos, M. Punk, *Phys. Rev. B* **95**, 024421 (2017).
[9] X. Bai, S.-S. Zhang, Z. Dun, H. Zhang, Q. Huang, H. Zhou, M. B. Stone, A. I. Kolesnikov, F. Ye, C. D. Batista, M. Mourigal, *Nature Physics* **17**, 467 (2021).
[10] S. M. Winter, A. A. Tsirlin, M. Daghofer, J. van den Brink, Y. Singh, P. Gegenwart, R. Valentí, *J. Phys.: Condens. Matter* **29**, 493002 (2017).
[11] D. H. Hurley, A. El-Azab, M. S. Bryan, M. W. D. Cooper, C. A. Dennett, K. Gofryk, L. He, M. Khafizov, G. H. Lander, M. E. Manley, J. M. Mann, C. A. Marianetti, K. Rickert, F. A. Selim, M. R. Tonks, J. P. Wharry, *Chemical Reviews* **122**, 3711 (2022).
[12] L. Desgranges, G. Baldinozzi, H. E. Fischer, G. H. Lander, *Journal of Physics: Condensed Matter* **35**, 10LT01 (2023).
[13] P. Santini, S. Carretta, G. Amoretti, R. Caciuffo, N. Magnani, G. H. Lander, *Rev. Mod. Phys.* **81**, 807 (2009).
[14] R. Caciuffo, G. Amoretti, P. Santini, G. H. Lander, J. Kulda, P. d. V. Du Plessis, *Phys. Rev. B* **59**, 13892 (1999).
[15] S. Carretta, P. Santini, R. Caciuffo, G. Amoretti, *Phys. Rev. Lett.* **105**, 167201 (2010).
[16] R. Caciuffo, P. Santini, S. Carretta, G. Amoretti, A. Hiess, N. Magnani, L.-P. Regnault, G. H. Lander, *Phys. Rev. B* **84**, 104409 (2011).
[17] R. Schönemann, G. Rodriguez, D. Rickel, F. Balakirev, R. D. McDonald, J. A. Evans, B. Maiorov, C. Paillard, L. Bellaiche, A. V. Stier, M. B. Salamon, K. Gofryk, M. Jaime, *Proceedings of the National Academy of Sciences* **118**, e2110555118 (2021).
[18] E. A. Tereshina-Chitrova, L. V. Pourovskii, S. Khmelevskyi, D. Gorbunov, R. Caciuffo, *Phys. Rev. B* **110**, 224417 (2024).
[19] B. T. M. Willis, *J. Phys. France* **25**, 431 (1964).
[20] B. T. M. Willis, R. I. Taylor, *Physics Letters* **17**, 188 (1965).
[21] B. C. Frazer, G. Shirane, D. E. Cox, C. E. Olsen, *Phys. Rev.* **140**, A1448 (1965).
[22] S. Nasu, *Japanese Journal of Applied Physics* **5**, 1001 (1966).
[23] J. Faber, G. H. Lander, *Phys. Rev. B* **14**, 1151 (1976).
[24] E. Blackburn, R. Caciuffo, N. Magnani, P. Santini, P. J. Brown, M. Enderle, G. H. Lander, *Phys. Rev. B* **72**, 184411 (2005).
[25] F. Bultmark, F. Cricchio, O. Grånäs, L. Nordström, *Phys. Rev. B* **80**, 035121 (2009).
[26] L. V. Pourovskii, S. Khmelevskyi, *Phys. Rev. B* **99**, 094439 (2019).
[27] S. Zhou, H. Ma, E. Xiao, K. Gofryk, C. Jiang, M. E. Manley, D. H. Hurley, C. A. Marianetti, *Phys. Rev. B* **106**, 125134 (2022).
[28] G. Amoretti, A. Blaise, R. Caciuffo, J. M. Fournier, M. T. Hutchings, R. Osborn, A. D. Taylor, *Phys. Rev. B* **40**, 1856 (1989).
[29] F. Zhou, V. Ozoliņš, *Phys. Rev. B* **83**, 085106 (2011).
[30] G. H. Lander, M. Sundermann, R. Springell, A. C. Walters, A. Nag, M. Garcia-Fernandez, K. J. Zhou, G. van der Laan, R. Caciuffo, *Journal of Physics: Condensed Matter* **33**, 06LT01 (2020).
[31] M. Sundermann, H. Hahn, D. S. Christovam, M. W. Haverkort, R. Caciuffo, B. Keimer, L. H. Tjeng, A. Severing, H. Gretarsson, *Phys. Rev. Res.* **7**, 043081 (2025).
[32] M. Dudzinski, J. Sznajd, *The European Physical Journal B - Condensed Matter and Complex Systems* **5**, 745 (1998).

[33] L. Desgranges, R. Caciuffo, H. E. Fischer, P. Garcia, G. H. Lander, Local atomic and magnetic order in uranium oxide at low temperature (doi:10.5291/ill-data.6-06-471), Institut Laue-Langevin (ILL) (2018).
[34] H. E. Fischer, G. J. Cuello, P. Palleau, D. Feltin, A. C. Barnes, Y. S. Badyal, J. M. Simonson, *Applied Physics A* **74**, s160 (2002).
[35] L. Desgranges, H. E. Fischer, G. H. Lander, G. Baldinozzi, *MRS Communications* **15**, 441 (2025).
[36] J. A. M. Paddison, J. Ross Stewart, A. L. Goodwin, *Journal of Physics: Condensed Matter* **25**, 454220 (2013).
[37] R. Brout, H. Thomas, *Physics Physique Fizika* **3**, 317 (1967).
[38] D. E. Logan, Y. H. Szczech, M. A. Tusch, *Europhys. Lett. (EPL)* **30**, 307 (1995).
[39] J. A. M. Paddison, *Phys. Rev. Lett.* **125**, 247202 (2020).
[40] J. A. M. Paddison, *Journal of Physics: Condensed Matter* **35**, 495802 (2023).
[41] G. H. Lander, J. Faber, A. J. Freeman, J. P. Desclaux, *Phys. Rev. B* **13**, 1177 (1976).
[42] A. M. Cook, S. Matern, C. Hickey, A. A. Aczel, A. Paramekanti, *Phys. Rev. B* **92**, 020417 (2015).
[43] S.-S. Diop, G. Jackeli, L. Savary, *Phys. Rev. B* **105**, 144431 (2022).
[44] J. A. M. Paddison, H. Zhang, J. Yan, M. J. Cliffe, M. A. McGuire, S.-H. Do, S. Gao, M. B. Stone, D. Dahlbom, K. Barros, C. D. Batista, A. D. Christianson, *npj Quantum Materials* **9**, 48 (2024).
[45] G. M. Wysin, *Phys. Rev. B* **62**, 3251 (2000).
[46] R. A. Cowley, G. Dolling, *Phys. Rev.* **167**, 464 (1968).
[47] M. E. Lines, E. D. Jones, *Phys. Rev.* **141**, 525 (1966).
[48] S. Toth, B. Lake, *J. Phys.: Condens. Matter* **27**, 166002 (2015).
[49] D. Dahlbom, H. Zhang, Z. Laraib, D. Pajerowsky, K. Barros, C. D. Batista, *arXiv:2304.03874* (2023).
[50] L. Paolasini, D. Chaney, A. Bosak, G. H. Lander, R. Caciuffo, *Phys. Rev. B* **104**, 024305 (2021).
[51] Y. Zheng, T. Lu, M. M. H. Polash, M. Rasoulianboroujeni, N. Liu, M. E. Manley, Y. Deng, P. J. Sun, X. L. Chen, R. P. Hermann, D. Vashaee, J. P. Heremans, H. Zhao, *Science Advances* **5**, eaat9461 (2019).
[52] Q. Wang, A. de la Torre, J. A. Rodriguez-Rivera, A. A. Podlesnyak, W. Tian, A. A. Aczel, M. Matsuda, P. J. Ryan, J.-W. Kim, J. G. Rau, K. W. Plumb, *Phys. Rev. X* **15**, 021021 (2025).
[53] A. Revelli, C. C. Loo, D. Kiese, P. Becker, T. Fröhlich, T. Lorenz, M. Moretti Sala, G. Monaco, F. L. Buessen, J. Attig, M. Hermanns, S. V. Streltsov, D. I. Khomskii, J. van den Brink, M. Braden, P. H. M. van Loosdrecht, S. Trebst, A. Paramekanti, M. Grüninger, *Phys. Rev. B* **100**, 085139 (2019).
[54] B. Hälg, A. Furrer, *Phys. Rev. B* **34**, 6258 (1986).
[55] P. A. Maksimov, A. L. Chernyshev, *Phys. Rev. Res.* **2**, 033011 (2020).